Nature of the density–magnetic-field-intensity correlation observed in the solar wind

Francesco Malara and Pierluigi Veltri
Dipartimento di Fisica, Università della Calabria, 87030 Arcavacata di Rende, Italy

Leonardo Primavera
Observatoire de Paris, 92195 Meudon, France

(Received 3 October 1996; revised manuscript received 5 March 1997)

A numerical model is set up to explain the observed behavior of the compressive fluctuations close to the heliospheric current sheet. The model assumes that large-amplitude Alfvén waves from the Sun enter the current sheet region producing a nonequilibrium state that evolves, giving rise to compressive fluctuations. The characteristics of the compressive fluctuations observed in our simulations reproduce in a detailed way how the correlation between the density and magnetic-field intensity depends on the fluctuation frequency, position with respect to the current sheet, and local β value in solar wind data. [S1063-651X(97)08908-3]

PACS number(s): 52.30.−q, 52.65.Kj, 96.60.Vg, 96.50.Ci

I. INTRODUCTION

When going from fast to slow speed streams in the solar wind, i.e., when approaching the heliospheric current sheet, the low-frequency fluctuations (1 min$<T<$1 day) display a completely different behavior. Alfvénicity, defined by the degree of correlation between velocity and magnetic-field fluctuations, decreases [1], while the level of density and magnetic-field-intensity fluctuations, which is very low in fast streams, considerably increases. Space data analyses have been performed to characterize these compressive fluctuations, mainly through the study of the correlation between proton density (δn) and magnetic-field intensity (δB) fluctuations. For instance, this correlation is positive (negative) in fast (slow) magnetosonic waves [2]. In particular, Vellante and Lazarus [3] have shown that for fluctuations at time scales larger (smaller) than $t_c \sim 10$ h, positive (negative) correlations prevail. More detailed analyses [4], which have been carried out in selected slow speed streams in the inner heliosphere, have shown that in some cases the correlation remains negative also at large scales.

Theoretical studies to explain the occurrence of a negative δn-δB correlation have been presented in the framework of ''nearly incompressible magnetohydrodynamics (MHD)'' [5–8]. Using this approach, the authors showed that for low and moderate Mach numbers, numerical simulations of turbulent flows, where the initial state consists of random equipartitioned solenoidal velocity and magnetic fluctuations, display a strong tendency to produce ''nearly incompressible'' solutions dominated by a negative δn-δB correlation. On the contrary, when starting with a random admixture of transverse and longitudinal velocity components, the density and magnetic amplitude are uncorrelated.

However, the above results apply to statistically homogeneous situations. In this paper we try to understand how compressive fluctuations are generated near the heliospheric current sheet, i.e., when fluctuations dynamically evolve in the presence of an inhomogeneous structure, such as a sheared magnetic field. Moreover, we will try to explain the occurrence of both the kind of observed δn-δB correlation and how this occurrence is related to the (i) fluctuation spatial scale, (ii) location with respect to the current sheet, and (iii) value of the plasma β.

A compressible numerical MHD model of the plasma around the heliospheric current sheet and of the fluctuations that are present in this region has been developed [9]. This model is based on the following arguments. In the solar wind, among Alfvénic fluctuations of solar origin, only those propagating away from the Sun should be found just beyond the critical point. Following those magnetic-field lines that converge on the two sides of the heliospheric current sheet, Alfvénic fluctuations enter the current sheet region. Then they are subject to a dynamical evolution, during which their characteristics drastically change; in particular, compressible fluctuations are produced. The main mechanisms driving the time evolution are related both to the inhomogeneity associated with the current sheet and to the opposite Alfvénic correlation of the fluctuations on the two sides of the current sheet. The results of the model [9] indicate that these mechanisms could be responsible for both the lack of Alfvénic correlation and the increased level of compressive fluctuations of slow speed streams.

In the present work we assume the model by Malara *et al.* [9], focusing on the correlation between density and magnetic-field intensity fluctuations. The results of the numerical simulations will be compared with the proton density–magnetic-field-intensity correlation calculated using the data set of some selected slow speed streams in the inner heliosphere.

The plan of the paper is as follows. In Sec. II the numerical model is described. In Sec. III the results of the model are presented and compared with solar wind data. In Sec. IV physical mechanisms that can determine the observed features are discussed.

II. NUMERICAL MODEL

The numerical model has been described already in a previous paper [9]; however, we report here its main characteristics. Our initial condition should represent a background magnetic field with a current sheet and large-amplitude fluctuations superposed: We assume that (a) the fluctuations are

Alfvénically correlated and propagate away from the Sun on both sides of the current sheet, (b) the total magnetic-field intensity (background plus perturbation) is uniform, and (c) the density and temperature are also uniform. Condition (b) ensures that dynamical effects induced by the ponderomotive force associated with $|\mathbf{B}|$ spatial variations are suppressed at the initial time. This kind of perturbation propagates without distortion in a uniform background magnetic field, but is subject to dynamical evolution when propagating in a current sheet.

To study the evolution of these initial conditions, we have solved the compressible MHD equations in the dimensionless form

$$\frac{\partial \rho}{\partial \tau}+\nabla\cdot(\rho\mathbf{v})=0, \tag{1}$$

$$\frac{\partial \mathbf{v}}{\partial \tau}+(\mathbf{v}\cdot\boldsymbol{\nabla})\mathbf{v}=-\frac{1}{\rho}\nabla(\rho T)+\frac{1}{\rho}\mathbf{j}\times\mathbf{b}+\frac{1}{\rho S_\nu}\nabla^2\mathbf{v}, \tag{2}$$

$$\frac{\partial \mathbf{b}}{\partial \tau}=\nabla\times(\mathbf{v}\times\mathbf{b})+\frac{1}{S_\eta}\nabla^2\mathbf{b}, \tag{3}$$

$$\frac{\partial T}{\partial \tau}+(\mathbf{v}\cdot\nabla)T+(\gamma-1)T(\nabla\cdot\mathbf{v}) =\frac{\gamma-1}{\rho}\left[\frac{1}{S_\kappa}\nabla^2 T+\frac{1}{S_\nu}\left(\frac{\partial v_i}{\partial x_j}\frac{\partial v_i}{\partial x_j}\right)+\frac{1}{S_\eta}\mathbf{j}^2\right], \tag{4}$$

where $\mathbf{j}=\nabla\times\mathbf{b}$ and $\gamma=5/3$ is the adiabatic index. Lengths are normalized to the shear length a, the magnetic field $\mathbf{b}$, and the mass density ρ to the respective characteristic values B_0 and ρ_0, the velocities to the Alfvén velocity corresponding to these values. The time τ, the pressure p, and the temperature T are normalized consistently. The quantities S_ν and S_η represent, respectively, the viscous and magnetic Reynolds numbers, while S_κ is a dimensionless number associated with the heat conductivity coefficient. Since dissipative coefficients are very low in solar wind we have used for the above quantities the largest values allowed by computer limitations: $S_\nu=S_\eta=S_\kappa/(\gamma-1)=1400$.

The considered geometry is $2\frac{1}{2}$ dimensional: All quantities depend on two space variables (x and y), but vector quantities have three nonvanishing components. Equations (1)–(4) have been numerically solved in a rectangular spatial domain $D=[-\ell,\ell]\times[0,\pi R\ell]$, with free-slip and periodic boundary conditions, along x and y, respectively. The x axis represents the cross-current sheet direction, while the y axis represents the propagation direction of the initial perturbation. The domain width ($2\ell=8$) has been chosen sufficiently larger than the shear length ($\simeq 1$), while the domain length is equal to the largest wavelength λ_{max} of the perturbation in the periodicity (y) direction. The aspect ratio has been chosen to be $R=0.15$, corresponding to $\lambda_{max}/a=3\pi/5$. The numerical technique is described elsewhere [10,9].

The total magnetic field at the initial time is given by

$$\mathbf{b}(x,y,0)=A\{\varepsilon\cos[\phi(y)]\hat{\mathbf{e}}_x+\sin(\alpha)F(x)\hat{\mathbf{e}}_y+\sqrt{1-\sin^2(\alpha)F^2(x)+\varepsilon^2\sin^2[\phi(y)]}\hat{\mathbf{e}}_z\}. \tag{5}$$

The function $F(x)$ is defined by

$$F(x)=\frac{\tanh x-\dfrac{x}{\cosh^2\ell}}{\tanh\ell-\dfrac{\ell}{\cosh^2\ell}}. \tag{6}$$

It monotonically increases with increasing x and is consistent with the free-slip boundary conditions at $x=\pm\ell$.

The equilibrium magnetic field $\mathbf{b}_{eq}(x)$ is obtained setting $\varepsilon=0$ in expression (5); it models the current sheet associated with a sector boundary of the solar wind. The magnetic field rotates by an angle 2α (we used $\alpha=\pi/4$ and $A=\sqrt{2}$) and its y component changes sign across the current sheet. The associated current $\mathbf{j}_{eq}$ is in the yz plane and its maximum is on the line $x=0$, where $\mathbf{j}_{eq}$ is in the z direction. The current sheet width is ~ 1; we will refer to the remaining part of the spatial domain as the ''homogeneous region.''

The perturbation amplitude has been chosen to be $\varepsilon=0.5$ and its spectrum is determined by the choice of $\phi(y)$. We used a power-law spectrum function

$$\phi(y)=2\sum_{m=1}^{m_{max}}(mk_0)^{-5/3}(\cos mk_0). \tag{7}$$

where $k_0=2\pi/\lambda_{max}$ and we have chosen $m_{max}=32$.

The fluctuating part δf of any quantity f is defined as

$$\delta f(x,y,\tau)=f(x,y,\tau)-\frac{1}{\pi R\ell}\int_0^{\pi R\ell} f(x,y,\tau)dy, \tag{8}$$

the solutions being periodic along the y direction. Using this definition to calculate the fluctuating part of the initial magnetic field (5), the initial velocity field is given by

$$\mathbf{v}(x,y,0)=\sigma(x)\frac{\delta\mathbf{b}(x,y,0)}{\sqrt{\rho(x,y,0)}}, \tag{9}$$

with $\sigma(x)=\tanh(x/\delta)$ and $\delta=0.05$. Expression (9) satisfy condition (a) everywhere, except in a thin layer around $x=0$, where $\sigma(x)$ changes sign. This choice of $\sigma(x)$ corresponds to a continuous change of the Alfvénic correlation sign from -1 to $+1$. This is necessary in order to have the same propagation direction of the initial Alfvénic perturbation on both sides of the current sheet, the y component of $\mathbf{b}_{eq}$ changing sign across the current sheet. The divergence of the initial velocity field is nonvanishing in the region where the correlation $\delta\mathbf{v}$-$\delta\mathbf{b}$ changes sign.

The initial density and temperature are

$$\rho(x,y,0)=1, \quad T(x,y,0)=T_0 \tag{10}$$

where T_0 is a free parameter of the model, which determines the sound velocity $c_s=(\gamma T_0)^{1/2}$ and the plasma β, defined by $\beta=c_s^2/c_A^2=\gamma T_0/A^2$. The plasma β represents a critical parameter with respect to the compressible fluctuation behavior. Then we have performed runs with three different values of β ($\beta=0.2$, run 1; $\beta=1$, run 2; and $\beta=1.5$, run 3).

III. RESULTS

Starting from the above initial condition, we have followed the time evolution of the system. In a short time ($\tau<1$) density $\delta\rho$ and magnetic-field-intensity δb fluctuations are generated, which spread in the transverse x direction, gradually filling the whole integration domain. The origin of such compressive fluctuations, which were not present in the initial condition, is due both to the interaction between the oppositely correlated Alfvénic perturbations on the two sides of the current sheet (represented by the initial nonvanishing divergence of the velocity field) and to the propagation of such Alfvénic perturbations in the inhomogeneity associated with the large-scale current sheet.

A detailed description of the time evolution of these compressive fluctuations has been presented elsewhere [9]. In the following we summarize the main features found in such fluctuations. The level of $\delta\rho$ and δb is higher in the current sheet region, where the sources of compressive fluctuations are located, than in the homogeneous region. Moreover, small-scale structures are generated, which are mostly localized within the current sheet. Actually, as a consequence of the above interaction mechanisms, in such a region the fluid is far from being in an equilibrium state. Compressive fluctuations with $\delta\rho$ and δb both correlated and anticorrelated have been detected. Among the latter, there are magnetic flux tubes (i.e., structures where the magnetic field is higher and the density lower than in the surrounding medium) and tangential discontinuities, both pressure balanced and quasistatic in the plasma reference frame, mostly concentrated in the current sheet region, where $\mathbf{b}_{eq}$ is quasiperpendicular to the propagation direction. Positively correlated $\delta\rho$-δb fluctuations, which belong to the fast magnetosonic mode, have been found propagating in oblique directions in the xy plane. The most intense among them form fast magnetosonic shocks, which gradually dissipate.

In the present work we focus on the correlation between the density and the magnetic-field-intensity fluctuations found in the simulation results, studying in particular the distribution of this correlation at different spatial scales. Moreover, since the correlation appears to change going from the current sheet to the homogeneous region, we studied its dependence on the transverse x direction. We define the density–magnetic-field-intensity correlation as

$$\sigma_{\rho b}=\frac{\langle\Delta\rho\Delta b\rangle_{\Delta x}}{\sqrt{\langle(\Delta\rho)^2\rangle_{\Delta x}\langle(\Delta b)^2\rangle_{\Delta x}}}, \tag{11}$$

where angular brackets indicate a running average taken over a length Δx,

$$\langle f\rangle_{\Delta x}=\frac{1}{\Delta x}\int_{-\Delta x/2}^{\Delta x/2} f(x+\xi,y,\tau)\,d\xi. \tag{12}$$

$\Delta f=f-\langle f\rangle_{\Delta x}$ represents the contribution of scales smaller than Δx (f being either ρ or b). Due to the symmetry of the problem, quantities have been periodically extended for $|x|>\ell$ in order to calculate the running average (12) also at points closer to the boundaries $x=\pm\ell$ than $\Delta x/2$.

Let us consider first the results of the low-β run ($\beta=0.2$, run 1). In Fig. 1 the correlation $\sigma_{\rho b}$ is plotted at the time $\tau=4.8$, i.e., several Alfvén times after the initial time. This quantity is represented as a function of the x coordinate, transverse to the current sheet, for a given value of y ($y=1.6$). From Fig. 1 we can see that, on average, positive (negative) correlations prevail in the whole domain at large (small) spatial scales Δx.

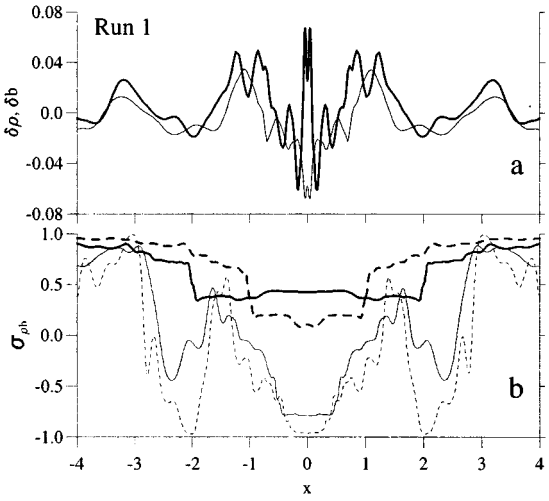

FIG. 1. Profiles of (a) $\delta\rho$ (thick line), δb (thin line), and (b) $\sigma_{\rho b}$ for $\Delta x=0.5$ (thin dashed line), $\Delta x=1$ (thin line), $\Delta x=2$ (thick dashed line), and $\Delta x=4$ (thick line) are shown as functions of x for $y=1.6$ and $\tau=4.8$, relative to run 1. All the quantities shown are dimensionless.

A closer examination reveals that, when going from the current sheet region to the homogeneous region, the correlation $\sigma_{\rho b}$ shows a different behavior at different scales. In particular, in the region close to the current sheet $\sigma_{\rho b}$ is slightly positive at scales $\Delta x\gtrsim 1$, while it is clearly negative for $\Delta x\lesssim 1$. In the homogeneous region $\sigma_{\rho b}$ is positive at large scales, while it does not show a definite sign at small scales. This behavior indicates that anticorrelated density–magnetic-field fluctuations, such as pressure balanced flux tubes and tangential discontinuities, prevail in the current sheet region. On the contrary, correlation corresponding to fast magnetosonic fluctuations dominate far from the current sheet at scales of the order of or larger than the current sheet width (which has been used as the normalization length in the present simulation).

A configuration with $\beta=1$ has been considered in run 2. Also in that case the interaction among the initial oppositely correlated Alfvénic fluctuations and the large-scale current sheet produces compressive perturbations with both positive and negative density–magnetic-field-intensity correlation. The former propagate transverse to the current sheet, filling the homogeneous region, while anticorrelated fluctuations remain dominant in the central region. In Fig. 2 the correlation $\sigma_{\rho b}$ is plotted, relative to run 2, for the same time as in Fig. 1. Around the current sheet region the behavior of $\sigma_{\rho b}$ is similar to that of the low-β run in that the correlation becomes increasingly negative with decreasing the scale Δx. Far from the current sheet $\sigma_{\rho b}$ is mainly positive. Comparing Figs. 1 and 2, it can be seen that the central region where a negative correlation is found is somewhat wider and $\sigma_{\rho b}$ more negative for $\beta=1$ than for $\beta<1$.

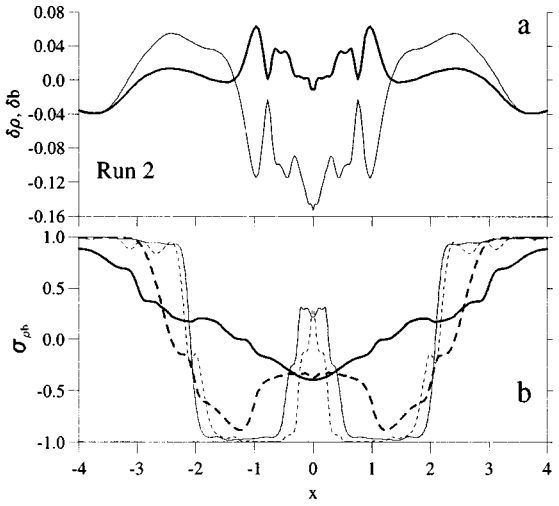

FIG. 2. Same as in Fig. 1, but for $y=1.0$, relative to run 2.

Finally, in run 3 we have considered a case with β larger than 1 ($\beta=1.5$). At variance with the previous runs, anticorrelated fluctuations rapidly expand out of the current sheet region, filling the whole spatial domain. After 4–5 Alfvén times a negative $\sigma_{\rho b}$ correlation dominates the whole structure. This situation is illustrated in Fig. 3, where the correlation $\sigma_{\rho b}$ is represented for the same value of τ as for Figs. 1 and 2. It can be seen that the correlation is strongly negative at any position and for all the considered spatial scales Δx, except for the smallest scale where localized spikes of a positive correlation are present.

We verified that the above-described features of $\sigma_{\rho b}$ shown in Figs. 1–3 remain essentially unchanged by changing the value of the y coordinate; then these figures are representative of what happens in the whole spatial domain. Moreover, the distribution of $\sigma_{\rho b}$ is calculated after several Alfvén times, when the above features of $\sigma_{\rho b}$ no longer display significant changes after the initial transient.

From Figs. 1–3 it is clear that the dependence of the correlation $\sigma_{\rho b}$ on both x and Δx, as it results from our model, is strongly influenced by the value of β. It is then

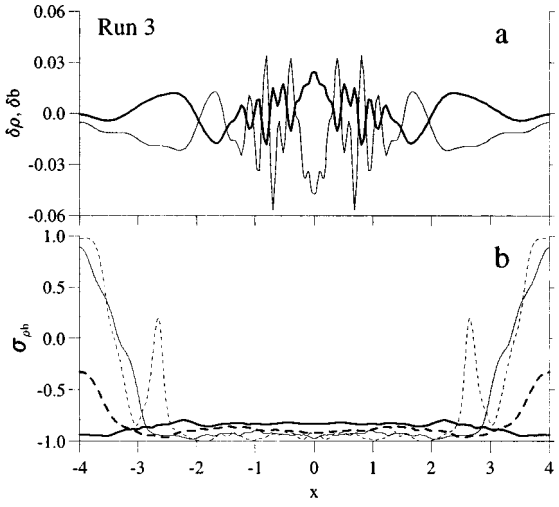

FIG. 3. Same as in Fig. 1, relative to run 3.

TABLE I. Quantities relative to the data in Figs. 4–7.

Parameters	Period 1	Period 2	Period 3	Period 4
$t_{start}-t_{end}$ (d)	72–74	45–47	54–56	101–103
R (AU)	0.69	0.905	0.85	0.32
$\langle n\rangle$ (cm^{-3})	~ 15	~ 8	~ 15	~ 140
$\langle T_e\rangle$ (K)	$\sim 1.5\times 10^5$	$\sim 1.5\times 10^5$	$\sim 1.5\times 10^5$	$\sim 3\times 10^5$
$\langle T_p\rangle$ (K)	$\sim 1\times 10^5$	$\sim 7\times 10^4$	$\sim 4\times 10^4$	$\sim 2\times 10^5$
$\langle B\rangle$ (nT)	~ 10	~ 7	~ 4	~ 28
$\langle\beta\rangle$	~ 1.1	~ 1	~ 5.1	~ 2.6
θ (deg)	18	43	34	29

interesting to see how these results compare with measures in slow speed streams of the solar wind, studying in particular the dependence of the proton density–magnetic-field-intensity correlation on the location (close to or far from the interplanetary current sheet), on the fluctuation scale, and on the value of the plasma β. For this comparison we used data taken by the Helios spacecraft in the inner heliosphere. We selected four periods, each one within a slow speed stream and containing crossings of the interplanetary current sheet. We will refer to these periods as periods 1–4. In Table I quantities relative to such data are collected: the initial and final time of the periods, the heliocentric distance R, the average proton density $\langle n\rangle$, the proton $\langle T_p\rangle$ and electron $\langle T_e\rangle$ temperatures, the magnetic-field intensity $\langle B\rangle$, and the corresponding average plasma beta $\langle\beta\rangle$. The latter quantity has been calculated using the expression

$$\langle\beta\rangle = 4\pi\gamma k_B \frac{\langle n\rangle(\langle T_e\rangle+\langle T_p\rangle)}{\langle B\rangle^2}. \tag{13}$$

It is worth noting that, during the considered periods, the quantities n, T_e, T_p, and B, as well as β, undergo fluctuations around the values listed in Table I. However, β ranges around 1 during periods 1 and 2, while β is significantly larger than 1 during periods 3 and 4.

We have calculated the proton density–magnetic-field-intensity correlation σ_{nB} during the above periods, at four different values of the time scale: $\Delta t=3$, 7, 13, and 25 h. Assuming a shear crossing time $t_a\sim 6$ h, the above values of Δt roughly correspond to the scale lengths Δx used in Figs. 1–3. The correlation σ_{nB} is plotted as a function of time in Figs. 4–7 for periods 1–4 (lower panels). In the upper panels the radial component v_R of the plasma velocity and the parallel magnetic-field component $B_\parallel(t)=\mathbf{B}(t)\cdot\hat{\mathbf{e}}_\parallel$ are plotted, $\hat{\mathbf{e}}_\parallel$ being the unit vector in the direction parallel to the current sheet. Such a direction has been calculated by the following procedure: In each of the four periods we have first determined the unit vector $\hat{\mathbf{e}}_\perp$, which is parallel to the ecliptic plane and minimizes the function

$$F(\hat{\mathbf{e}}_\perp)=\sum_i (\mathbf{B}_i\cdot\hat{\mathbf{e}}_\perp)^2. \tag{14}$$

The sum in Eq. (14) is extended over data contained into the given period, sufficiently far from the current sheet. The vector $\hat{\mathbf{e}}_\perp$ roughly gives the direction normal to the current sheet projected onto the ecliptic plane. Note that the same proce-

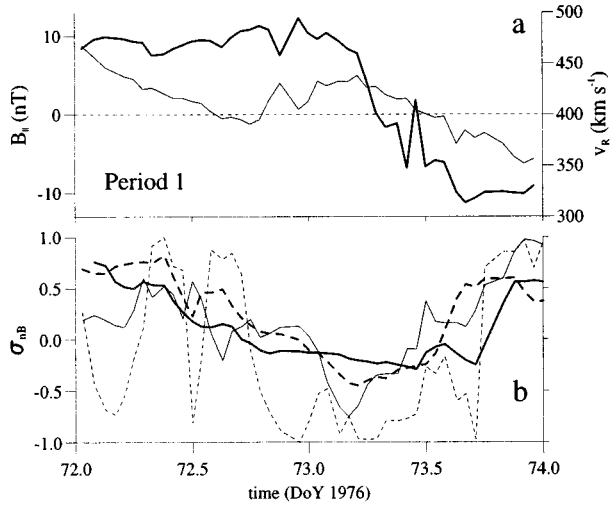

FIG. 4. Profiles of (a) the magnetic-field parallel component (full line), the velocity radial component (dashed line), and (b) the correlation σ_{nB} for $\Delta t=3$ h (thin dashed line), $\Delta t=7$ h (thin line), $\Delta t=13$ h (thick dashed line), and $\Delta t=25$ h (thick line), as functions of time, relative to period 1. (DOY stands for day of year.)

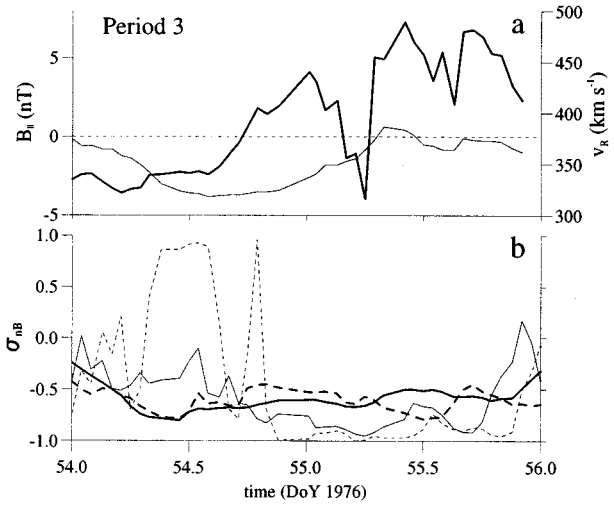

FIG. 6. Same as Fig. 4, relative to period 3.

dure applied to the equilibrium structure of the simulation gives $\hat{\mathbf{e}}_\perp=\hat{\mathbf{e}}_x$, the unit vector normal to the current sheet. Then the vector $\hat{\mathbf{e}}_\parallel$ is calculated as perpendicular to $\hat{\mathbf{e}}_\perp$ and parallel to the ecliptic plane. The values of the angle θ between $\hat{\mathbf{e}}_\parallel$ and the radial direction, relative to the four periods, are given in Table I. The plots of the parallel component $B_\parallel$ of Figs. 4–7 are useful in determining the location of the current sheet crossings during the four periods.

Let us consider first the plots of Fig. 4, which correspond to a $\beta\sim 1$ period (period 1) during which only one current sheet crossing took place. Close to the current sheet the correlation σ_{nB} becomes more negative with decreasing time scale Δt. Outside that region σ_{nB} is definitely positive at all the time scales, except for the smallest one ($\Delta t=3$ h), for which σ_{nB} has a less defined sign. The plots of Fig. 4 compare well with the results of the $\beta\leqslant 1$ runs shown in Figs. 1 and 2: The above-described dependence of the proton density–magnetic-field-intensity correlation on both location (close to or far from the current sheet) and time scale (Δt) during period 1 displays the same behavior as that found in the results of runs 1 and 2.

During period 2 the value of β ranges also around 1, but the data set contains several crossings of the current sheet, which are quite close to one another. As a consequence, the pattern of the correlation σ_{nB} (Fig. 5) is more complex than for period 1. However, also in period 2, close to the current sheet crossings the correlation becomes more negative with decreasing time scale Δt. Getting far from the current sheet, the correlation tends to become larger, at least for intermediate time scales. Then, also in that case the results of the low-β run reproduce the correlation σ_{nB}, though the comparison is somewhat less clear because of the presence of a multiple current sheet crossing.

The value of β is larger than 1 during periods 3 and 4. In such cases the correlation σ_{nB} appears to be definitely negative at all the considered time scales (Figs. 6 and 7) and is more negative than in periods 1 and 2. At the smallest time

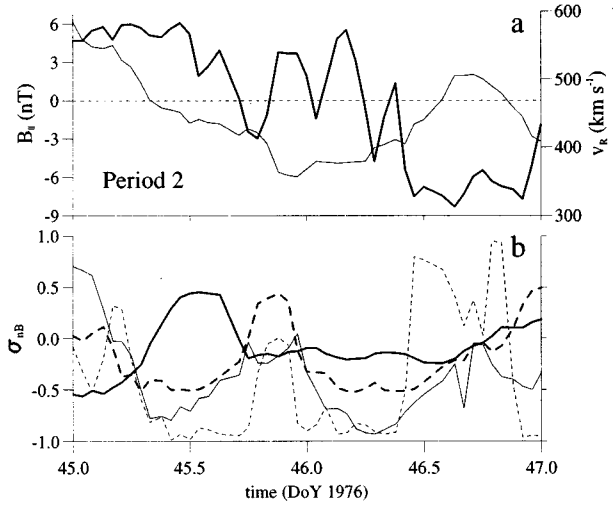

FIG. 5. Same as Fig. 4, relative to period 2.

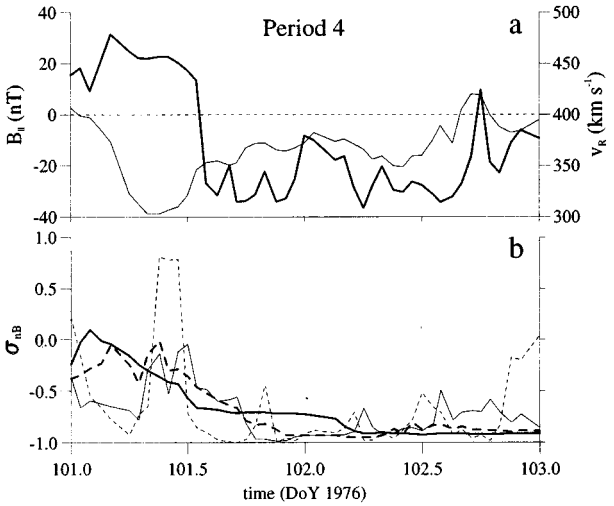

FIG. 7. Same as Fig. 4, relative to period 4.

scale the correlation sporadically rises to large positive values. The location of current sheet crossings seems not to affect the correlation σ_{nB}. Comparing with the results of run 3, it can be seen that both the dominant negative correlation and the spikes of the positive correlation at the smallest scale are reproduced by the numerical model.

IV. DISCUSSION AND CONCLUSION

We have developed a model for the generation of compressive MHD fluctuations in solar wind slow speed streams. In our model we assume that two streams of Alfvénic fluctuations, both propagating away from the Sun, converge on the two sides of the heliospheric current sheet following the magnetic lines. Two mechanisms are responsible for the formation of compressive fluctuations.

(a) The equilibrium magnetic field has opposite directions on the two sides of the current sheet, thus the two streams of Alfvénic perturbations have an opposite $\delta\mathbf{v}$-$\delta\mathbf{B}$ correlation. Since div$\mathbf{B}=\mathbf{0}$, then div$\mathbf{v}$ cannot be vanishing in the location where the Alfvénic correlation changes sign; this represents a source of compressions in the region where the two opposite correlated fluctuations come into contact.

(b) The inhomogeneity associated with the large-scale current sheet couples Alfvénic perturbations with compressive modes [11]; thus the energy of the initial Alfvénic perturbation is partially transferred to density and magnetic-field-intensity fluctuations.

Both mechanisms are at work in the current sheet region and destroy the noncompressive Alfvénic character of the initial perturbation. In particular, the latter is active during the whole time evolution. We studied the density–magnetic-field-intensity correlation $\sigma_{\rho b}$ as it is produced in our model by the above mechanisms. We found that $\sigma_{\rho b}$ depends on the location x, on the spatial scale Δx, and on the value of the plasma β. We have tried to compare the results of the model with the proton density–magnetic-field-intensity correlation σ_{nB} in solar wind slow speed streams considering four samples of the Helios spacecraft data set.

We have found that the dependence of σ_{nB} on location (close to or far from the current sheet), on the fluctuation scale, and on the value of β are qualitatively reproduced by the numerical model. It is worth noting that in the data sets considered β shows important fluctuations around the average value, while it is assumed to be uniform in the numerical model. Moreover, at variance with the model that includes only one current sheet, multiple current sheet crossings are present in three of the four samples. In fact, the correlation found in the $\beta\leqslant 1$ runs compares better with the σ_{nB} found in period 1 (single current sheet crossing) than in period 2 (multiple current sheet crossing). For the above reasons, a more detailed comparison between the results of the model and the Helios data set would be beyond the aim of the present work.

The similarity between simulation results and solar wind data shows that the main physical mechanisms that determine the density–magnetic-field-intensity correlation observed in slow speed streams have been included in our numerical model. This allows us to try to give a physical interpretation for the n-B correlation observed in the vicinity of the heliospheric current sheet. Density and magnetic-field fluctuations, both positive and negative correlated, are produced around the current sheet by the above-described mechanisms, but in order to escape from that region they must propagate at large angles with respect to the background magnetic field. Actually, close to the current sheet the background magnetic field is mainly perpendicular to the cross-current sheet direction. This fact represents a limitation for the propagation of negatively-correlated fluctuations; indeed, slow magnetosonic perturbations (which are characterized by anticorrelated ρ and $|\mathbf{B}|$ fluctuations) have a vanishing phase velocity when the wave vector is perpendicular to the background magnetic field, so they tend to remain confined close to the current sheet. On the contrary, this limitation does not affect positively-correlated fluctuations, which are free to propagate away from the current sheet. As a consequence, the region around the current sheet will be dominated by negative-correlated compressive structures with wave vectors nearly perpendicular to the large-scale magnetic field (flux tubes and tangential discontinuities).

Since the above mechanisms produce compressive fluctuations inside the current sheet, in such a region the level of compressive fluctuations is higher and nonlinear effects are more intense than outside. Then a nonlinear cascade is produced [9] that transfers negatively correlated fluctuations toward small scales. This could explain why σ_{nB} becomes more negative with decreasing scale Δt in the current sheet region. Outside such a region, positively correlated compressive fluctuations (fast mode) propagating away from the current sheet are essentially present. For this reason, moving away from the current sheet σ_{nB} becomes positive, at least at large scales and in situations with $\beta\lesssim 1$.

When $\beta>1$, both in solar wind data and in our simulation negatively correlated fluctuations are observed also outside the current sheet; moreover, negative correlation prevails at all time scales. This could be related to the tendency of a magnetofluid with $\beta>1$ to develop compressive structures in which magnetic and gas pressure fluctuations are anticorrelated. Actually, in the current sheet region the interaction between the initial Alfvénic perturbation and the large-scale inhomogeneity generates both magnetic pressure and density fluctuations. If the sound velocity is larger than the Alfvén velocity, such density perturbations can propagate sufficiently fast to balance the magnetic pressure fluctuations by opposite gas pressure fluctuations. This argument, which has been invoked by Roberts and Wiltberger in a different context [12] and is at the basis of the occurrence of negative correlation in the nearly incompressible solution at high β [5–8], could explain why anticorrelated n-B fluctuations are more frequent than positively correlated fluctuations, for β sufficiently larger than 1.

In conclusion, the present model indicates that the n-B correlation in the solar wind slow speed streams is determined by both the presence of the heliospheric current sheet and the value of the average β. Concerning the latter point, let us note that Marsch and Tu [4] calculated the spectrum of the proton density-magnetic pressure n-p_b correlation for three slow speed streams, at distances from the Sun $R=0.31$, 0.69, and 0.89 AU. Such streams contain period 4, period 1, and period 2, respectively. Each spectrum of Marsch and Tu is calculated on the whole stream, so there is no information about the dependence of the n-p_b correlation

on the location. However, from Fig. 3 of [4] it appears clearly that the n-p_b correlation behaves in a completely different way according to the value of β; in particular, the n-p_b correlation is negative in the high-β stream (0.31 AU), while in the two $\beta \sim 1$ streams it goes from positive to negative values with increasing frequency. These behaviors are consistent with those shown in Figs. 7, 4, and 5, respectively.

We finally note that all of the dynamical evolution in our model takes place in few unit times. Since time is normalized to the Alfvén time $t_A = a/c_{A0} = (1/2)(2a/v_{sw})(v_{sw}/c_{A0})$, assuming $c_{A0} \sim 70$ km s^{-1}, $v_{sw} \sim 350$ km s^{-1}, and $2a/v_{sw} \lesssim 12$ h (the time that the spacecraft takes to cross the current sheet), we find $t_A \lesssim 30$ h, i.e., most of the time evolution of the simulation takes place in the inner heliosphere.

ACKNOWLEDGMENTS

The authors are grateful to R. Bruno for valuable discussions about the subject of the paper. This work is part of a research program that is financially supported by the Ministero dell'Università e della Ricerca Scientifica e Tecnologica; the Consiglio Nazionale delle Ricerche, Contract No. 94.00802.CT02; the Agenzia Spaziale Italiana, Contract No. 94-RS-164; and the CEE Human Capital and Mobility program, Contract No. ERBCHRXCT930410.

[1] J. W. Belcher and L. Davis, J. Geophys. Res. **76**, 3534 (1971).
[2] A. I. Akhiezer, I. A. Akhiezer, R. V. Polovin, A. G. Sitenko, and K. N. Stepanov, *Plasma Electrodynamics* (Pergamon, New York, 1975), Vol. 1.
[3] M. Vellante and A. J. Lazarus, J. Geophys. Res. **92**, 9893 (1987).
[4] E. Marsch and C. Y. Tu, Ann. Geophys. **11**, 659 (1993).
[5] W. H. Matthaeus and M. R. Brown, Phys. Fluids **31**, 3634 (1988).
[6] W. H. Matthaeus, L. W. Klein, S. Ghosh and M. R. Brown, J. Geophys. Res. **96**, 5421 (1991).
[7] G. P. Zank and W. H. Matthaeus, J. Geophys. Res. **97**, 17 189 (1992).
[8] G. P. Zank and W. H. Matthaeus, Phys. Fluids A **5**, 257 (1993).
[9] F. Malara, L. Primavera, and P. Veltrip, J. Geophys. Res. **101**, 21 597 (1996).
[10] F. Malara, J. Comput. Phys. **124**, 254 (1995).
[11] F. Malara, L. Primavera, and P. Veltri, Astrophys. J. **459**, 347 (1996).
[12] D. A. Roberts and M. J. Wiltberger, J. Geophys. Res. **100**, 3405 (1995).